BNL-220886-2021-JAAM

Integrative investigation of dust emissions by dust storms and dust devils in North Africa

L. Pan, Y. Liu

To be published in "Science of The Total Environment"

February 2021

Environmental and Climate Sciences Department

Brookhaven National Laboratory

U.S. Department of Energy

USDOE Office of Science (SC), Biological and Environmental Research (BER) (SC-23)

DISCLAIMER

Integrative investigation of dust emissions by dust storms and dust devils in North Africa

Lin Pan [a,b], Yongxiang Han [a,*], Zhengqi Lu [a], Jiaxin Li [a], Fei Gao [a,c], Zhaohuan Liu [a], Weijia Liu [a,d], Yangang Liu [d]

[a] *Collaborative Innovation Center on Forecast and Evaluation of Meteorological Disasters, Nanjing University of Information Science and Technology, Nanjing 210044, China*
[b] *Zhoushan Meteorological Bureau, Zhoushan 316000, China*
[c] *Inner Mongolia Meteorological Service Center, Inner Mongolia 010051, China*
[d] *Brookhaven National Laboratory, Upton, NY, USA*

HIGHLIGHTS

- Two dust emission mechanisms in North Africa are studied and quantified.
- Dust storms mainly occur in Spring with dust emission regions in northern and north-eastern.
- Dust devils mainly occur in Summer with dust emission regions in the center of North Africa.
- The annual emissions from dust storms and dust devils contribute 61.3% and 38.7% to the total dust emission, respectively.

GRAPHICAL ABSTRACT

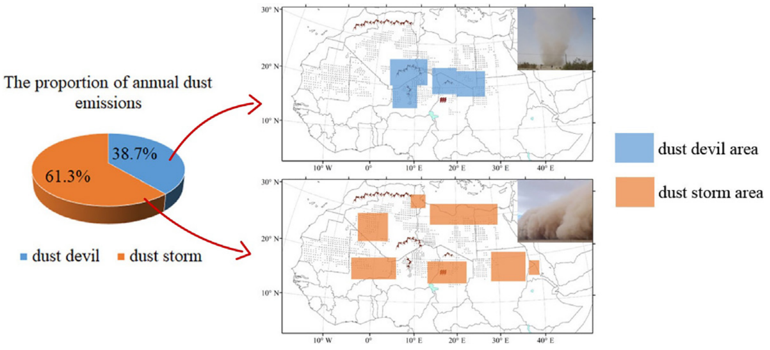

ABSTRACT

Dust aerosols in North Africa account for >50% of the global total; however dust emission areas are still unclear. Based on the analysis of dust storms simulated with the numerical Weather Research and Forecast (WRF) model, satellite aerosol index (AI), and the dust data observed at 300 meteorological stations over 20 years, the spatio-temporal distribution characteristics of dust storm, dust devil and AI are compared and analyzed. The results show that: 1) There are two dust emission mechanisms: the dynamically-dominated dust storm and thermally-dominated dust devil; 2) Dust storms occur most frequently in Spring and are concentrated in the areas of Grand Erg Occidental Desert to the Erg Chech-Adrar Desert, the northern part of Grand Erg Oriental, the Atouila Desert to the Ouarane Desert, the Mediterranean coast, the eastern side of Nubian Desert and Bodélé Depression; 3) Dust devils occur most frequently from April to August and are mainly concentrated in the central part of North Africa, especially in the southwest of Hoggar Mountains to the west of Air Mountains, the border area of Egypt - Sudan - Libya and the vicinity of Tibesti Plateau; 4) The spatio-temporal distribution of AI is cor-related more with the dust devils emission whereas the annual average contributions by dust storms and dust devils are 61.3% and 38.7%, respectively. This study discovers a new area of dust emissions by dust devils, and pro-vides a better explanation for the spatio-temporal distribution of AI in North Africa.

1. Introduction

Dust aerosols contribute more than half of the total atmospheric aerosols in the troposphere (IPCC, 2013), and have a significant impact on the climate through direct effect (Maley, 1982), indirect effect

Nomenclature

DAE_{tot}	total dust devil emission
D_{time}	duration of the dust devil
S_t	grid area where the dust devil's instantaneous position is located
σ	fractional area covered by a dust devil
F_d	average dust flux in a dust devil flux
μ	dimensionless coefficient for the turbulent dissipation of mechanical energy
η	thermodynamic efficiency
ΔP	air pressure difference from the surface to the tropopause
ρ_{air}	air density
g	acceleration of gravity
Z_{CBL}	boundary layer height
T_R	radiation time scale of the convective boundary layer
F_{in}	heat flow of the dust devil
Γ_{ad}	adiabatic lapse rate
T_h	ground temperature

(Alpert et al., 1998), and iron fertilizer effect (Watson et al., 2000; Martin, 1990). They have gradually become a key link between the global material cycle, climate and environmental change (Ridgwell, 2007; Wang et al., 2015; Perlwitz et al., 2001; Obianyo, 2019; Oo et al., 2019; Solangi et al., 2019).

North Africa, located on both sides of the North Return Line, covers an area of 8.37 million square kilometers with the world's largest mo-bile desert and the Sahara Desert. As the world's largest dust emission area, dust emission there provides about 500 million to 1 billion tons of dust aerosols to the atmosphere every year, accounting for >50% of the global dust aerosols.

However, due to the sparsity of meteorological observation stations, the dust research in this area is relatively weak compared to that in other areas, with sporadic investigation on dust emission area and di-vergent conclusions. At present, the identification of dust emission area relies mainly on three methods: meteorological observation, satel-lite aerosol index, and numerical simulations. Bertrand et al. (1979) in-ferred, by analyzing the visibility and wind direction data from 27 meteorological stations in South Sahara, that Mauritania and Bilma in Nigeria were located at or near dust emission areas. Kalu (1979) con-firmed Bertrand's supposition using the dust track analysis, and identi-fied the Faya largeau area on the western slope of Tibesti Plateau as an important dust emission area in North Africa. Wang et al. (2011) ana-lyzed the spatial distribution of dust storm frequencies in North Africa using one-year observational data. They concluded that the Sahara de-sert and Sahel are not only the main dust emission area in North Africa, but also the largest dust emission area in the world, with the most frequent dust storm events occurring in Spring. Based on the hourly visibility data at 53 meteorological stations in West Africa, N'Tchayi et al. (1997) concluded that the Sahel replaced central Sahara as the main dust emission area in North Africa, with the Bodélé Depres-sion being by far the largest dust emission area. Used the satellite aero-sol index, Brooks and Legrand (2000) identified Bodélé Depression as an important source region, together with a large swathe of country cover-ing portions of Mauritania, Mali and southern Algeria. In addition, the Horn of Africa, the Nubian Desert in southern Egypt, and Northern Sudan are also important areas of dust emission. Prospero et al.(2002) and Washington et al. (2003) further determined the Bodélé Depression as a Sahara Desert as well as the world's most important dust emission area. Goudie and Middleton (2001) considered Western Sahara also as an important dust emission area in addition to Bodélé Depression. Mahowald et al. (2002) argued that the Chad Lake had be-come an important potential dust emission area due to the exposure of nearly 20,000 km^2 of lake sediments (Birkett, 2000), with the Lake Chad source's contribution being negligible compared to the Bodélé Depres-sion, which is about 700 km north of the Lake (Prospero et al., 2002; Washington et al., 2003). Using dust storm models, Mokhtari et al.(2015) simulated the annual average dust emission in the Sahara from 2006 to 2010 using ALADIN combined with ORILAM aerosol scheme, which showed that the annual average dust flux in the Bodélé Depres-sion is the highest (2 kg·m^{-2}·year^{-1}), followed by central Niger (400–-600 g·m^{-2}·year^{-1}), Grand Erg Occidental and Grand Erg Oriental in Algeria, the Western Sahara coast, the central of Mauritania and Mali (200–400 g·m^{-2}·year^{-1}), and southeastern region of Libya and Sudan, and along the border between Egypt and Libya (100–200 g·m^{-2}·year^{-1}). Using satellite infrared images and a dust storm model, Evan et al. (2015) determined that 82% of the dust emission in North Africa comes from the 15–20°N Sahel, with most of the dust emissions coming from the Bodélé Depression (64% ± 16%) and the depression (13% ± 3%) lying in the lee of the Air and Hoggar Mountains.

A comparison of North African dust emission areas identified by three methods - meteorological observations, satellite aerosol index and numerical modelling of dust storm - reveals both common emission areas (e.g., the Sahel) and a large number of different emission areas. In particular, the emission area identified by the satellite aerosol index (AI) differs significantly from those determined by meteorological observa-tions and dust storm models. The core reason is that AI reflects the total amount of all dust aerosols, which includes dust aerosols triggered by strong winds (e.g., dust storms), weak winds (e.g., dust devils), and long-range transports.

However, previous studies by use of meteorological observations and dust storm models have only considered the cases of strong winds, and assumed that dust emission is a non-linear function of wind speed with a wind threshold of 5 m/s for dust emission (Helgren and Prospero, 1987). In addition, although North Africa exhibits the most frequent dust storms in the world, the average dust storm days per year observed by most weather stations is <3 days, suggesting that the dust storm process is an event of small probability. Thus the an-nual and monthly AI will smooth out some of the real dust emission areas. For example, the low annual and monthly AI in Sahara would imply that the Sahara was not a dust emission area, contradicting with the conclusions based on meteorological observations. Furthermore, the time of high AI values (Summer) does not exactly match that of the dust storm occurrence (Spring) time. Similar phenomenon also oc-curs in the deserts of Northern China, where AI remains high during the months when dust storms are rare (Wang et al., 2012). Liu et al. (2018) compared the dust emission and deposition in Tengger Desert from 2006 to 2015, and found that in most days without dust weather, the dust deposition remained high for the same period. These results sug-gest the existence of an additional dust emission mechanism that have been overlooked in previous studies.

Unlike the dynamically-dominated dust storms that require strong winds, the dust emission by dust devils is predominantly thermal. Dust devils occur in sunny, weakly windy weather conditions due to the uneven heating of the surface (Gu et al., 2003; Gu et al., 2010). Han et al. (2008) argued that dust devils first carry dust aerosols into air, and the thermal convection continuously transports the fine dust particles up to the top of the boundary layer. Through observations and simulations of dust devils in the northern deserts of China, Han et al. (2016) concluded that dust devil's emission accounts for more than half of the annual total dust emission and was an important source of atmospheric dust aerosols. Due to the difficulty to directly observe the basic parameters of the dust devil, the study on dust devil emissions has relied mainly on numerical simulations. Klose and Shao (2016) sim-ulated the dust devils' distribution and their contribution to the annual dust emission in Australia using Large Eddy Simulation. The authors be-lieved that the dust emission by dust devils was underestimated by the simulation. Jemmett-Smith et al. (2015) introduced a method to deter-mine the occurrence of dust devils based on many meteorological factor thresholds. Tang et al. (2018) applied this method with modified the meteorological factor thresholds for dust devil occurrence based on the observations of the meteorological variables related to the dust devil in the deserts of Northern China. They further proposed a param-eterization for the dust devil emission, and coupled it with the WRF model. The simulated dust devil occurrence pattern, region, and dust emission matched well with the observations, and the calculated dust devil emission represented 53% of the total annual emission.

Based on the previous studies, there are at least two dust emission mechanisms: by dynamically-dominated dust storms and by thermally-dominated dust devils. The meteorological observations and simulations of dust storm weather processes only reflect the dust emission driven by strong winds. However, AI is a composite index of the total amount of dust aerosols produced by the various local dust emission mechanisms and remote transports. To address the deficiencies, here we combine the three methods to conduct an integrative investigation of dust emissions. The daily AI in North Africa from 1997 to 2016 is used to determine the total dust emission. The relationship between the sum of emissions by storms and devils and AI is quantified, and the dust emission areas in North Africa are determined. Further, the contributions of dust storms and dust devils to the total emission are quantified by analyzing the observations collected at 300 stations, and simulations of WRF with the dust devil parameterization. The study reveals new dust emission areas by dust devils, and reconciles the discrepancy between the spatio-temporal distribution of AI and dust storms.

The rest of the paper is organized as follows. Section 2 describes the area of study, data sources and methods. Section 3 presents the results. Main conclusions are summarized in Section 4.

2. Study area, data sources and methods

2.1. Study area

North Africa is located on both sides of the northern tropic with flat terrains. Controlled by the subtropical high pressure zone with dry and hot sinking air, the region's main climate types are Mediterranean and tropical desert, with the world's largest desert — the Great Sahara Desert, consisting of nearly 17 deserts (Fig. 1). In addition, there are four large mountains: Atlas Mountains (1000-4165 m, ASL) in the northwest of north Africa, Hoggar Mountains (3003–4627 m, ASL), Air Mountains (>1300 m, ASL) and Tibesti Plateau (2000 m, ASL) with a peak of 3415 m in the central part of North Africa. A narrow strip of 320-480 km wide in the south of the Sahara Desert (about 10–15°N and known as the Sahel) experiences annual precipitation of 200 mm to 800 mm from north to south, an arid and semi-arid zone in the transi-tion from African savannah to Sahara Desert. As shown in Fig. 1, there are a total of 300 meteorological stations in the study area, mainly dis-tributed in southwestern North Africa with more developed river sys-tems, the Nile Basin and northern North Africa. A few sites are located in the outer edge of the desert.

(A: Grand Erg Occidental B: Grand Erg Oriental C: Edeyen Ubari D: Erg Calnascio E: Erg Libyan F: Erg Rebiana G: Edeyen Murzuq H: Erg Chech-Adrar I: Erg Iguidi J: Erg Maurit K: Erg Djouf L: El Mréyé M: Erg Atouila N: Erg Tombuctou O: Erg Ouarane P: Erg Tenere Q: Grand Erg de Bilma R: Erg Djourab S: Erg Nubian)

2.2. Data sources

The meteorological and dust data at the 300 meteorological stations are from the North African surface international exchange stations ac-quired from the National Meteorological Information Center of China. The AI data are from the NASA TOMS and OMI satellites. Reanalysis data are NCEP and NCAR (https://www.esrl.noaa.gov/psd/cgi-bin/data/composites/printpage.pl). The time series of data are from January 1997 to December 2016.

2.3. Description of model and numerical setup

The Weather Research and Forecasting (WRF) model is a mesoscale prediction model system jointly developed by the environmental pre-diction center of the National Oceanic and Atmospheric Administration (NOAA) and the National Atmospheric Research Center (NCAR) of the

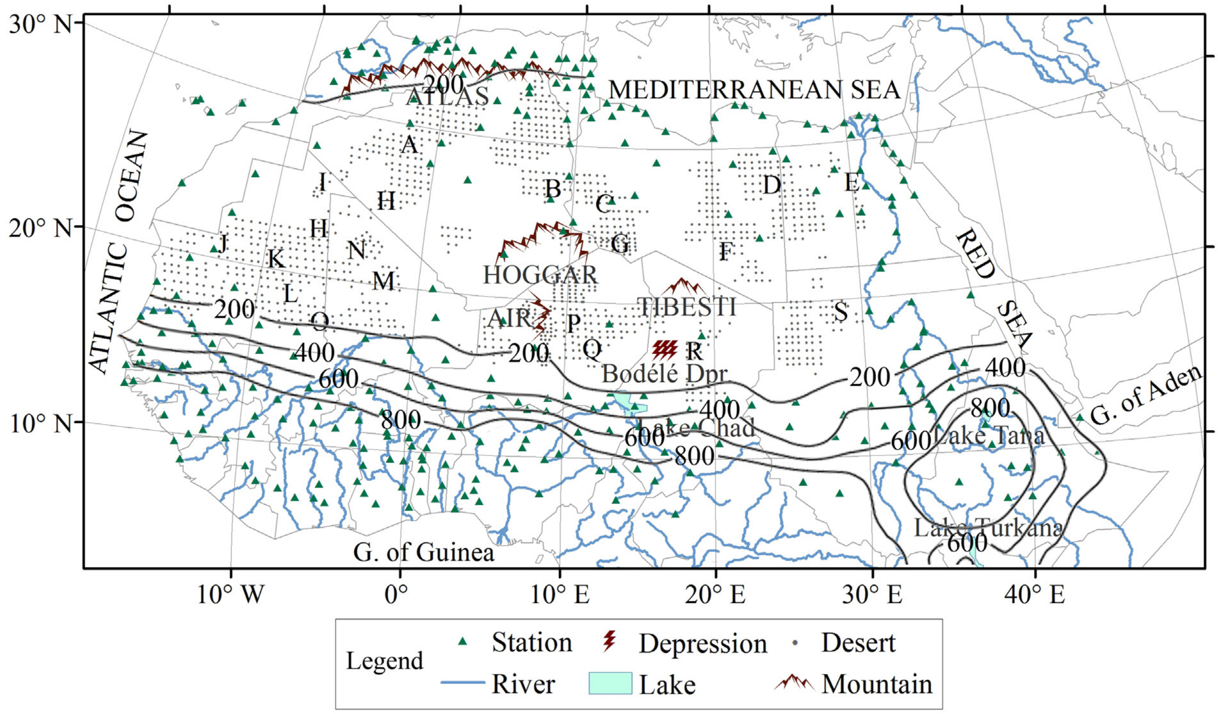

Fig. 1. North Africa landforms, annual precipitation (mm), and distribution of meteorological stations.

United States. We uses WRFV3.6.1 in this study that considers the pro-cess of dust emission, transmission and settling. The simulation spans about two decades from January 1997 to December 2016 with outputs every 6 h. The NCEP/NCAR reanalysis data with a time resolution of 6 h and 1° × 1° are used as the initial and boundary conditions.

The model adopts one layer of nesting; the simulation domain (0°N ~ 40°N, 20°W ~ 50°E) with 60 × 150 grids and a horizontal spacing of 50 km and 33 vertical layers from the ground to 50 hPa is employed. The terrain data uses the 2 m and 30s high-resolution LANDUSE data provided by USGS. The related physical parameterization schemes are as follows: Lin scheme for cloud microphysics, YSU scheme for bound-ary layer, Noah scheme for land surface, Monin-Obukhov scheme for surface layer, RRTMG scheme for both short-wave and long-wave radi-ation, GOCART scheme for dust storm.

A dust devil occurrence scheme based on five meteorological factor thresholds (Tang et al., 2018). The five factor thresholds are: 1) Wind Erosion Index >0 as a dust emission area; 2) near-surface (0–2 m) adi-abatic decline rate (LR) ≥ 8.5 K/m (Jemmett-Smith et al., 2015); 3) the ratio of convective buoyancy w^* to friction velocity $u^* > 5$ (Lyons et al., 2008; Oke et al., 2007; Jemmett-Smith et al., 2015); 4) ambient wind speed is between 2 and 7 m/s (Ansmann et al., 2009); 5) no dust devils when the cloud threshold >7 or when there is precipitation (Tang et al., 2018).

2.4. Calculation of dust devil emission

The total dust devil emission (DAE_{tot}) is calculated with

$$DAE_{tot} = D_{time} \times S_t \times \sigma \times F_d \tag{1}$$

where D_{time} is the duration of the dust devil; S_t is the area where the dust devil's instantaneous position is located (Sinclair, 1969; Balme and Greeley, 2006; Oke et al., 2007); F_d is the average dust flux in a dust devil flux of 0.7 g/(m^2·s) (Metzger, 1999; Gillette and Sinclair, 1990); The fractional area σ covered by a dust devil is estimated by Koch and Renno (2005):

$$\sigma = \left(\frac{\mu}{\eta}\right)^{1/2} \left(\frac{\Delta P}{\rho_{air} g T_R}\right)^{3/2} \left(\frac{F_{in}}{\rho_{air}}\right)^{-1/2} \tag{2}$$

where $\mu = 18$ is the dimensionless coefficient for the turbulent dissipa-tion of mechanical energy; $\rho_{air} = 1.29$ kg/m^3 is the air density; $g = 9.8$ m/s^2 is the gravitational acceleration; $T_R \approx 9 \times 10^5$ s is the radi-ation time scale of the convective boundary layer; $F_{in} \approx 155$ W/m^2 is the heat flow of the dust devil; the air pressure difference from the surface to the boundary layer top is $\Delta P = \rho_{air} g Z_{CBL}$ with Z_{CBL} being the boundary layer height; the thermodynamic efficiency η is given by (Koch and Renno, 2005):

$$\eta = \frac{\Gamma_{ad} Z_{CBL}}{T_h} \tag{3}$$

with $\Gamma_{ad} = 10$ K/km, and T_h being the adiabatic lapse rate and the ground temperature, respectively.

2.5. Analysis workflow

For convenience, Fig. 2 illustrates the general workflow of our anal-ysis. First, by simulating the emissions of dust storms and dust devils at each grid point, the spatio-temporal distributions of the dust emissions from both are obtained, and compared with the number of dust storms days from 300 weather stations. Second, the spatio-temporal distribu-tions of the emission sum by storms and devils are compared and

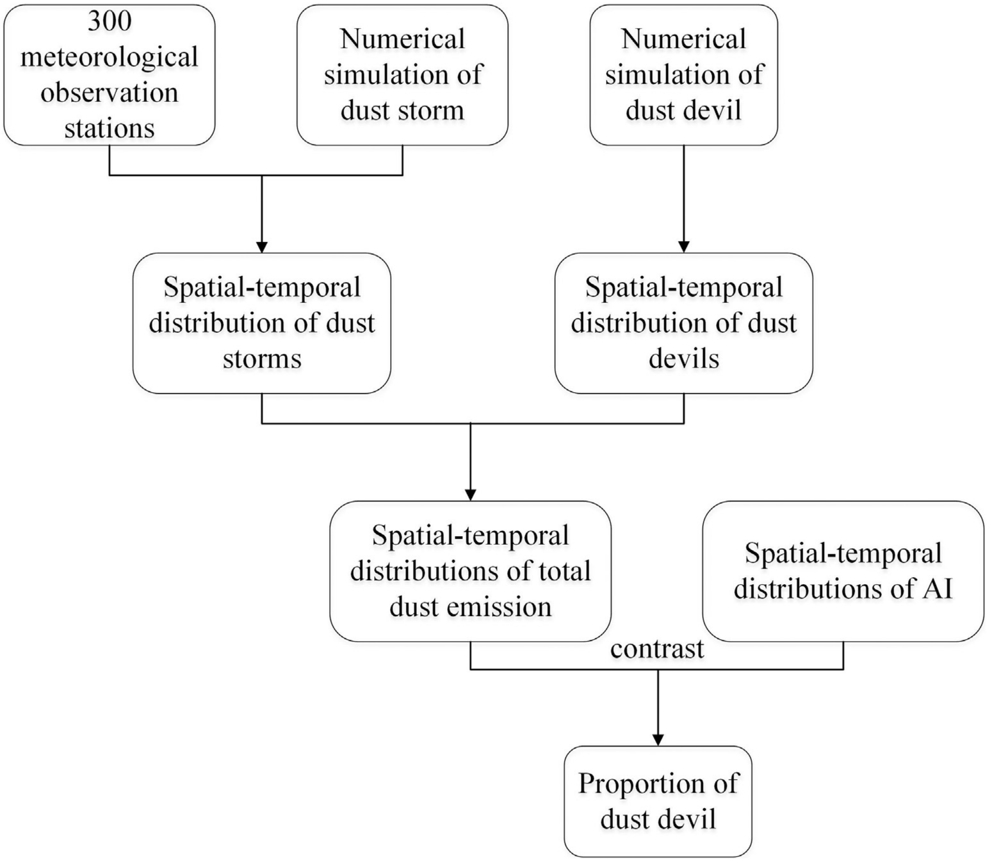

Fig. 2. Illustration of analysis workflow.

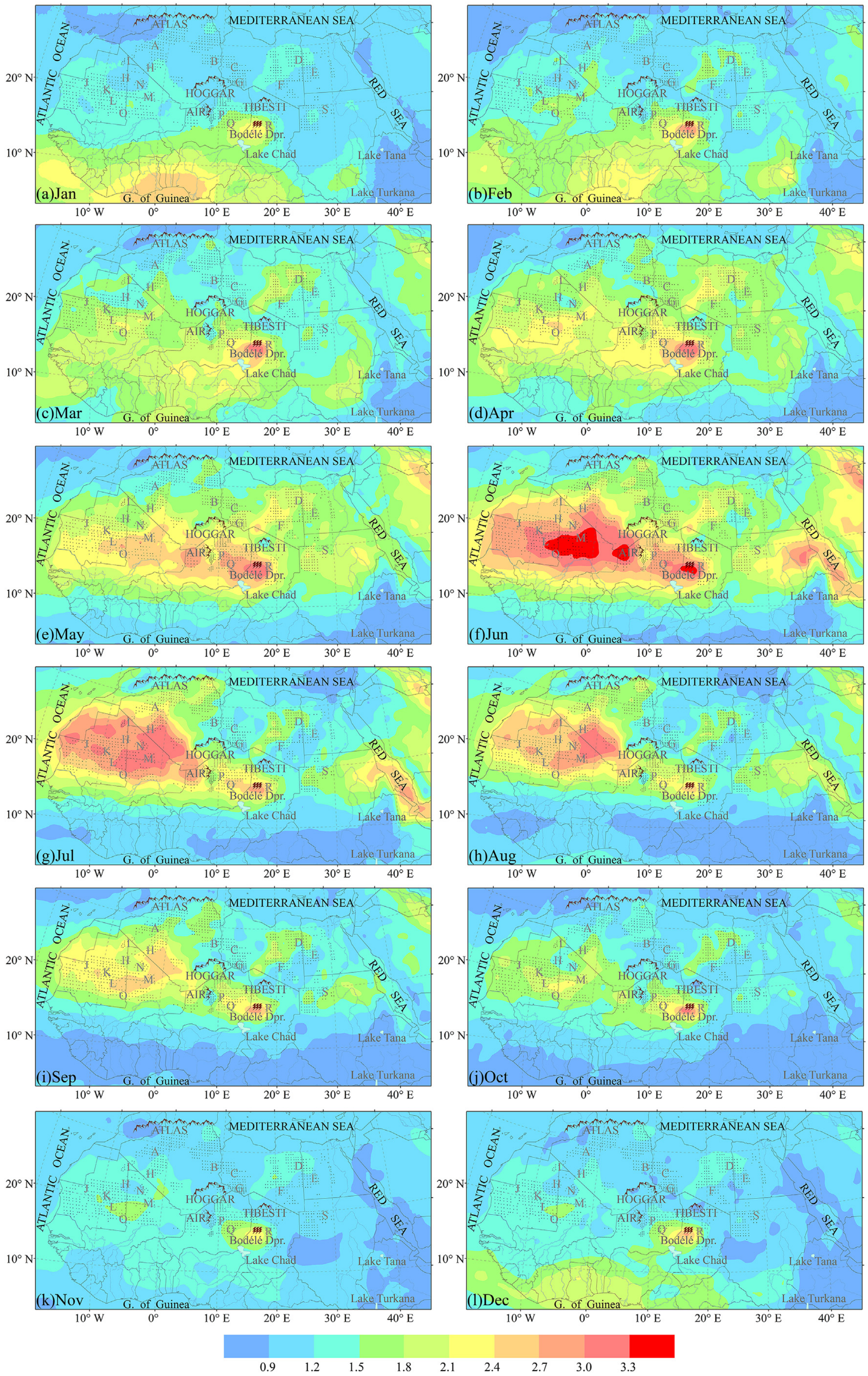

Fig. 3. Monthly spatial distribution of AI in North Africa averaged over the period of 1997 to 2016.

analyzed with that of AI. Finally, the contribution of dust devils to dust emission sum is obtained.

3. Results

3.1. AI-based dust emission areas

The satellite aerosol index (AI) is used as an indicator of the total dust amount, because anthropogenic aerosols are minimal in North Africa and the data are not available. The spatial distribution of the 20-year average AI for each month in North Africa (Fig. 3) shows that the areas with AI <1.5 almost cover North Africa and can be regarded as background aerosol. In December, the high-value areas where AI is con-sistently >1.5 are located in both the Gulf of Guinea and Bodélé Depres-sion at 0–10°N. In January, the AI high-value area in the Gulf of Guinea begins to strengthen and expand northward, and connects with the high-value area in the Bodélé Depression. From February to June, this high-value area gradually extends northward and eastward to the whole Sahel region and Sahara Desert. And by June, both regional ex-pansion and the intensity of high-value areas are maximized, forming four regional centers with AI >3.0: near the Atouila Desert and the Ouarane Desert, the west of the Air Mountains, the Bodélé Depression and east of the Nubian Desert. With the expansion of the region and the increase of the intensity, the high-AI region moves northward as a whole, and the AI over the south Sahel returns to the background value. From July to November, the high-value areas begin to gradually shrink and diminish in intensity, although the areas continue to move northward. By November, AI remains high value between 2.1 and 2.4 only for the Bodélé Depression. It is noteworthy that from June to July there is an obvious small area of high AI (up to 3.0 or higher) in the northern part of Eritrea bordering Sudan, and this high-AI area begins to decrease until August. The AI value at the Bodélé Depression is above 2.1 throughout the year.

3.2. Dust emission areas revealed by dust storm simulation and observation

Fig. 4 shows the spatial distribution of annual average dust emissions simulated in this study (a) and simulated by Mokhtari et al. (2015) using the ALADIN model of coupled SURFEX surface parameter-ization scheme from 2006 to 2010 (b). Both results show that the areas of high dust emissions are located in the Bodélé Depression, northern Western Sahara, along the Mediterranean Sea and Southeast Nubian Desert, with the dust emissions simulated in this paper is slightly lower than that of Mokhtari et al. (2015).

(a: this paper from 1997 to 2016; b: Mokhtari et al. (2015) from 2006 to 2010)

The monthly spatial distribution of the average dust storm emissions (Fig. 5) shows that the simulated areas of dust emissions are largely fixed, mainly concentrated in six independent regions: the Grand Erg Occidental and Erg Chech-Adrar, the northern part of Grand Erg Orien-tal, the Mediterranean coast, the eastern side of the Nubian Desert, the Atouila Desert and Ouarane Desert, and Bodélé Depression, while the Hoggar Mountain, Air Mountain, Tibesti Plateau and the southern side of Calnascio Desert at about 20°N have almost no dust emissions and not dust source areas. In terms of the spatial distribution by month, the dust emissions have the least amount from September to November, with the exception of the Bodélé Depression, where it is lower than 10 g/m^2. Dust storm emissions begin to increase gradually from Decem-ber onwards, with the Bodélé Depression being particularly notable, reaching up to 30 g/m^2. The dust storm emissions in all regions show a significant increase trend in January, which continues to increase from February and March, with the highest emission >30 g/m^2. From April to May, the emissions continue to increase except in the Bodélé Depression where it decreases significantly. In June, except for the northern part of Eritrea where it increases slightly, all other regions show a decreasing trend, especially in the Bodélé Depression where the amount decreases to 14-18 g/m^2. In July, the emission rising in the northern part of Western Sahara is >30 g/m^2, while the emission in-creases rapidly in northern Eritrea and becomes a new high-value area, reaching above 30 g/m^2, as in northern Western Sahara. In addi-tion, the emission in other areas continues to decrease. In August, the dust storm emission in North Africa begins to decrease as a whole, while the high-value zone in northern Eritrea remained with no signif-icant change in the emission intensity. In September, this high-value re-gion decreases sharply or even almost disappear.

Compared with the dust storm days by 300 meteorological stations and other study (Pan et al., 2020), the simulated high-emission areas roughly coincide with high dust storm days, and the simulated high-value areas are mostly located in the desert hinterland while the ob-served high values are on its outer edge, implying that the unobserved desert hinterland has more dust activity than its outer edge, which is consistent with common sense and implies that the simulation dust emission map is more refined. Combined the observed dust storm days and simulation results, the dust storms occur mainly north of 15°N, and their dust storm emission areas are mainly concentrated in the northern part of the Grand Erg Oriental, the Grand Erg Occidental to the Chech Desert, the Mediterranean coast, the eastern side of the Nu-bian Desert, the Atouila Desert to the Ouarane Desert, and the Bodélé Depression is the most important dust emission area in North Africa. However, the Hoggar Mountains, Air Mountains, Tibesti Plateau and the south side of Calnascio Desert at about 20°N are not dust storm emission areas.

Although Figs. 3 and 5 show some similarities between the daily dust storm emission and the daily AI from 1997 to 2016 in North Africa with a correlation coefficient of 0.29 and significance $\alpha = 0.0001$, in depth analysis reveals more discrepancies. Firstly, high dust storm area ex-tends southward from the northern North Africa from December to April, while the AI high-value area extends southward

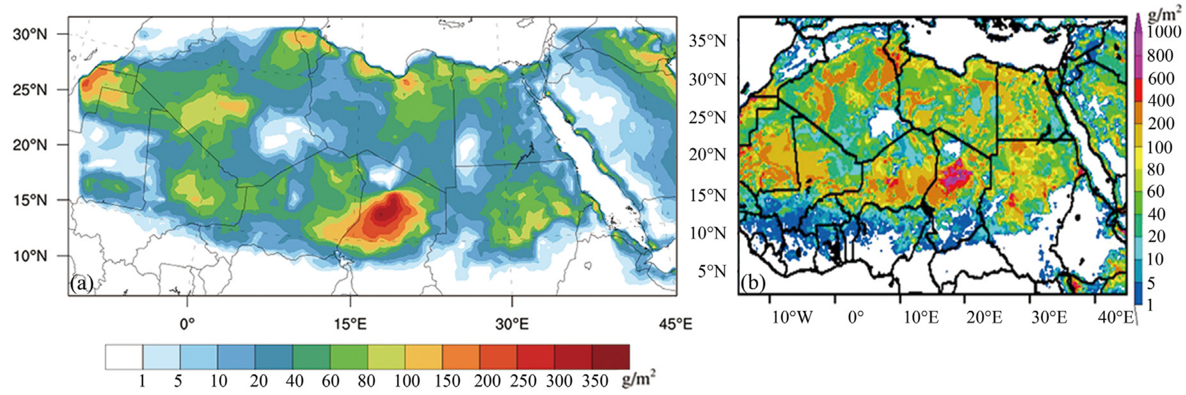

Fig. 4. Simulated spatial distribution of annual dust emission in North Africa.

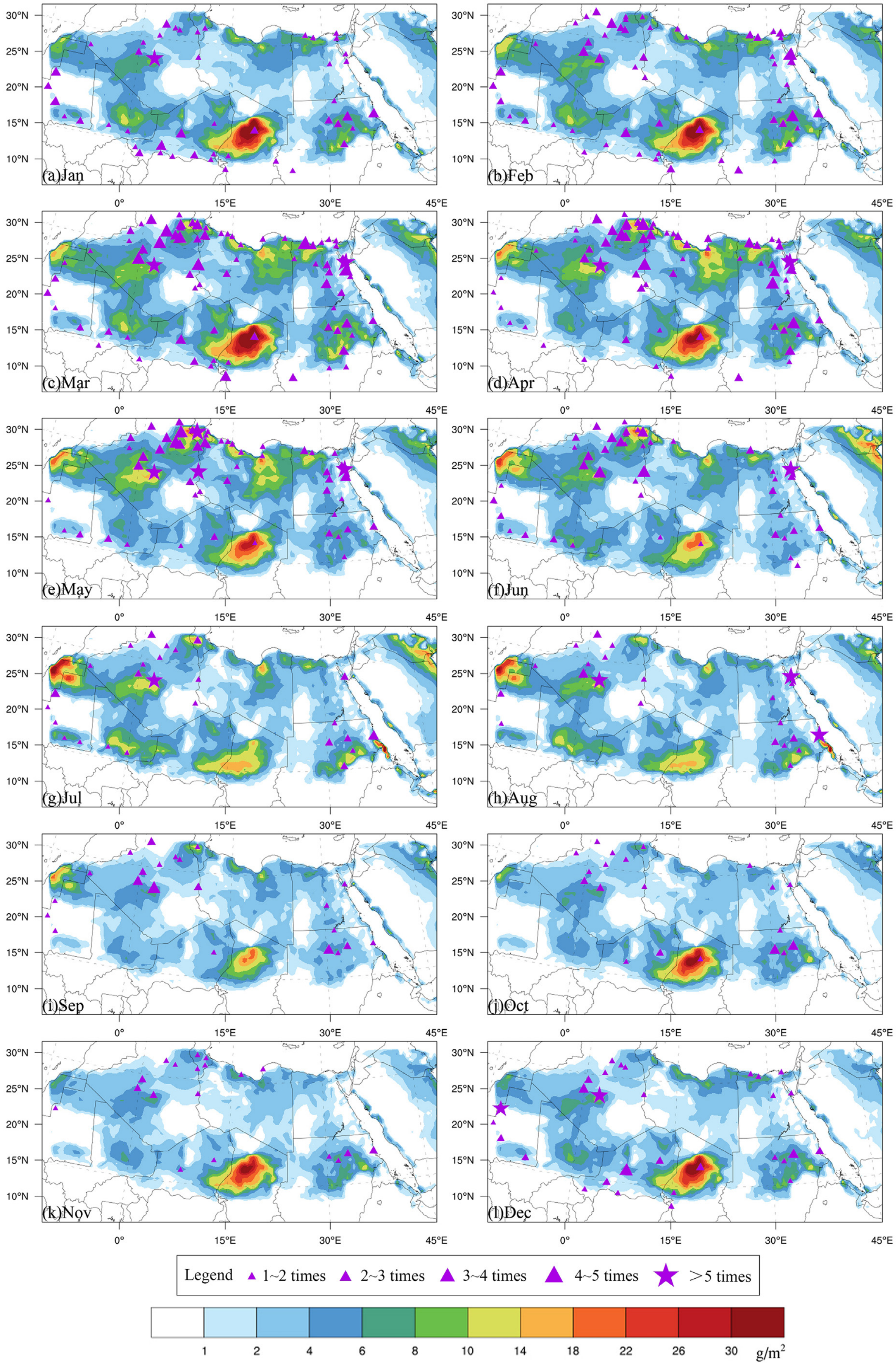

Fig. 5. Spatial distribution of the simulated monthly averages of dust storm emissions and days from weather stations in North Africa from 1997 to 2016.

southern North Africa from December to August, and their high-value areas overlapped in the Sahel and the Sahara Desert during April to Au-gust, with very small overlapped areas in the rest of the time. Secondly, dust storm mostly occurs in Spring, but AI has higher values from May to August, and they do not match in the timing of high values occurrence. Thirdly, according to the dust storm observation and simulation results, the Hoggar Mountains, Air Mountains, Tibesti Plateau and the southern side of Calnascio Desert are not the dust source area, but the AI value from the southwest of Hoggar Mountains to the west of Air Mountains from February to October was always above 1.5, peaking at over 3.3 in June; the AI value around Tibesti Plateau begins to gradually increase from February onwards, reaching 1.8 in June; the southern part of Calnascio Desert has AI values higher than 1.5 from April to June. These results imply that the monthly or yearly averaged AI may not fully reflect the dust aerosol emitted by dust storms.

(The triangle represents the weather station where dust storm is ob-served, and its size represents different days of dust storm per year. The pentagram represents the station where dust storms occur for more than five days a year)

3.3. Dust emission areas revealed by simulated dust devils

The spatial distribution of dust emission by dust devils by month over 20 years in North Africa (Fig. 6) shows that the dust emission is very low from October to January, only a few regions have 2–6 g/m^2. The emissions begin to increase from February and are mainly concen-trated in the Sahel south of 20°N. In contrast to February's a few scattered emission areas, March's emission areas rapidly expand and become contiguous in the Sahel, with the areas concentrated in the south of Sahel, Air Mountains, Tibesti Plateau and the southeast side of Djourab Desert. The dust emissions range between 10 and 14 g/m^2. From April to July, the emission areas expand rapidly northward to 30°N, along with a significant increase in emission amount, and the dust aerosols are mainly concentrated in the south of the Hoggar Moun-tains and south of the Sahel. The area where the largest emission amount reaching 26 g/m^2 is located near the Air Mountains. In May, the areas continue to expand northward to the Mediterranean coast; the high-emission areas in the Air Mountains and Tibesti Plateau con-tinue to enhance, up to 30 g/m^2 near the Air Mountains; but the emis-sions begin to decrease to lower than 14 g/m^2 in the southern Sahel at south of 15°N. June's emissions do not change significantly from May, but the area in the western North Africa begins to shrink and the Djouf desert is almost no dust emission; the high-emission area near Tibesti Plateau extends eastward to the south of Calnascio Desert where emission amount reaches 10–14 g/m^2. In July, the emission areas and amount decrease further in western North Africa, but the areas in eastern North Africa expand to the Red Sea coast. At the same time, there is a marked increase in dust emission in northern and central North Africa, and the range above 10 g/m^2 has significantly increased, especially in the vicinity of the Hoggar Mountains, the western Air Mountains, the Tibesti Plateau and the Egypt - Sudan - Libya border areas, where it reaches up to 26 g/m^2. August's emission areas and amounts both begin to decrease, but there is still an obvious high-emission area near the Tibesti Plateau where emission amount can reach 22–26 g/m^2. September's emission areas shrink rapidly towards the center of North Africa, and the emission amount also decreases rap-idly to 2–10 g/m^2 over most of the areas. There are only a few scattered emission areas in the west of Air Mountains and Tibesti Plateau in Octo-ber, leaving only one in the western Air Mountains in November, and there is almost no dust emission area in December.

In summary, the dust emission by dust devils mainly occurs from April to August, and the dust devil emission areas are mainly concentrated in the central North Africa north of 10°N, especially in the south-west of the Hoggar Mountains to the west of the Air Mountains, the border area of Egypt - Sudan - Libya and the vicinity of the Tibesti Plateau.

Comparative study of Figs. 6 and 3 shows that the trend of the two are almost identical, and the high-value regions are both characterized by a northward expansion from southern North Africa. In particular, the dust emission regions revealed by dust devils and that by AI highly coincide with each other from April to August. In addition, the AI high-value areas occur southwest of the Hoggar Mountains to the west of the Air Mountains and near the Tibesti Plateau, where there are no dust storms but a high occurence of dust devils, implying that the dust emis-sion in these areas is likely to be dominated by the dust devils. In addi-tion, the daily dust devil emissions from 1997 to 2016 have a significant positive correlation with daily AI, with the correlation coefficient of 0.69 is much higher than that of 0.29 between AI and dust storm emissions for the same sample size. The result suggests that the monthly spatial distribution of AI is more reflective of dust devil emissions than dust storm emissions.

3.4. Simulated monthly spatial distribution of sum of emission by storms and devils versus AI

Atmosphere dust aerosols have at least two mechanisms of dust emission, the dynamically-dominated dust storm and the thermally-dominated dust devil. Fig. 7 shows the simulated monthly spatial distri-bution of the mean sum of emission by dust storms and dust devils over the 20 years. Evidently, the sum of dust emission from October to No-vember is several scattered areas, such as the Mediterranean coastline, the northern part of Western Sahara, Grand Erg Occidental to the Chech Desert and the eastern side of the Nubian Desert, where the sum is very small, and the area larger than 10 g/m^2 is mainly concen-trated in Bodélé Depression. From December to January, the sum starts to increase, and Bodélé Depression expends above 30 g/m^2, but the dust emission areas are still scattered. The scattered areas begin to connect in February, and they are almost united by March, and the sum has further increased. From April to May, the sum increases significantly in the vi-cinity of Air Mountains, the Grand Erg Occidental to the Chech desert, the northern part of Western Sahara and along the Mediterranean. At the same time, the sum around the Tibesti Plateau has also increased significantly and is connected to the high-emission area of Bodélé De-pression. June's sum begin to decrease near the Air Mountains and Bodélé Depression, but continue to increase in the northern part of Western Sahara, and the high-emission area around the Tibesti Plateau begins to expand to the southern part of Calnascio Desert. July's sum in the northern part of Western Sahara reaches the highest of the year, and continues to increase along the Hoggar Mountains - Tibesti Plateau -Calnascio Desert line, while a new high-emission area has been formed in northern Eritrea. There is no significant change in the dust emission area in August compared with July, but the sum of dust emission inten-sity is obviously weakened, and in September, the sum of dust emission area is obviously reduced towards central of North Africa, with the emission intensity decreasing to a maximum of 22 g/m^2, while the dust emission area in northern Eritrea have disappeared.

A comparison of the monthly spatial distribution of AI with that of the sum of dust emission in North Africa shows that, although the sum of dust emission does not move northward gradually from the Gulf of Guinea as shown by AI since December, but their spatial change along time is very similar. Both have an annual minimum from October to November, an increasing trend from December onwards, an annual maximum from June to July, and a decrease after July. The Bodélé De-pression, the area from the southwestern Hoggar Mountains to the western Air Mountains and the northern Eritrea correspond very well.

Although the spatial distributions of the sum of dust emission and AI are similar in general, they still do not fully overlap in details, such as the Atouila Desert and Ouarane Desert have higher AI but smaller dust emission. Near the Tibesti Plateau, the dust emission is high from March to September, while AI is high only from April to June and in a slightly smaller range. These facts suggest that although the two dust emission mechanisms above can roughly explain the spatial distribution

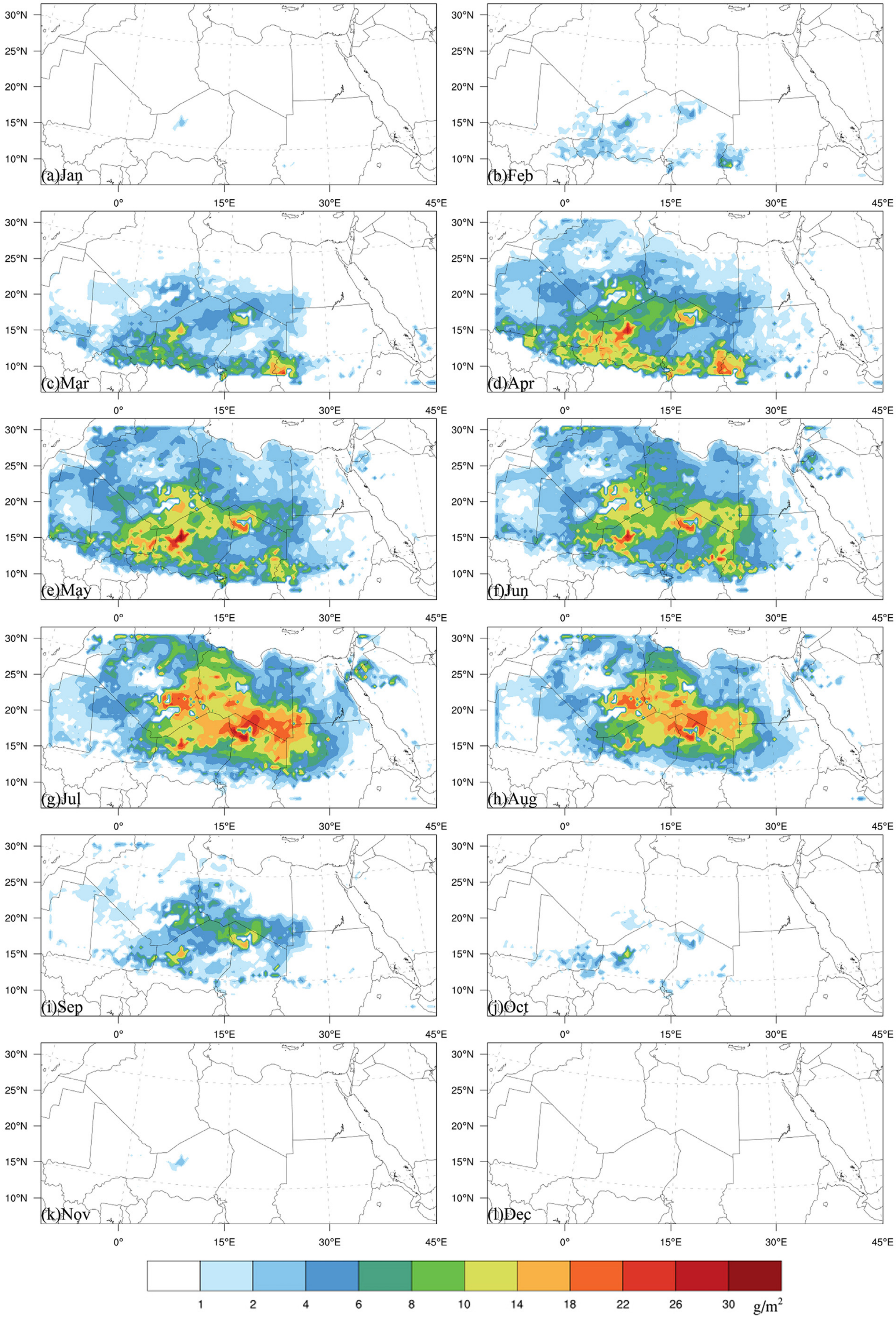

Fig. 6. Spatial distribution of the simulated monthly averages of dust devil emissions in North Africa from 1997 to 2016.

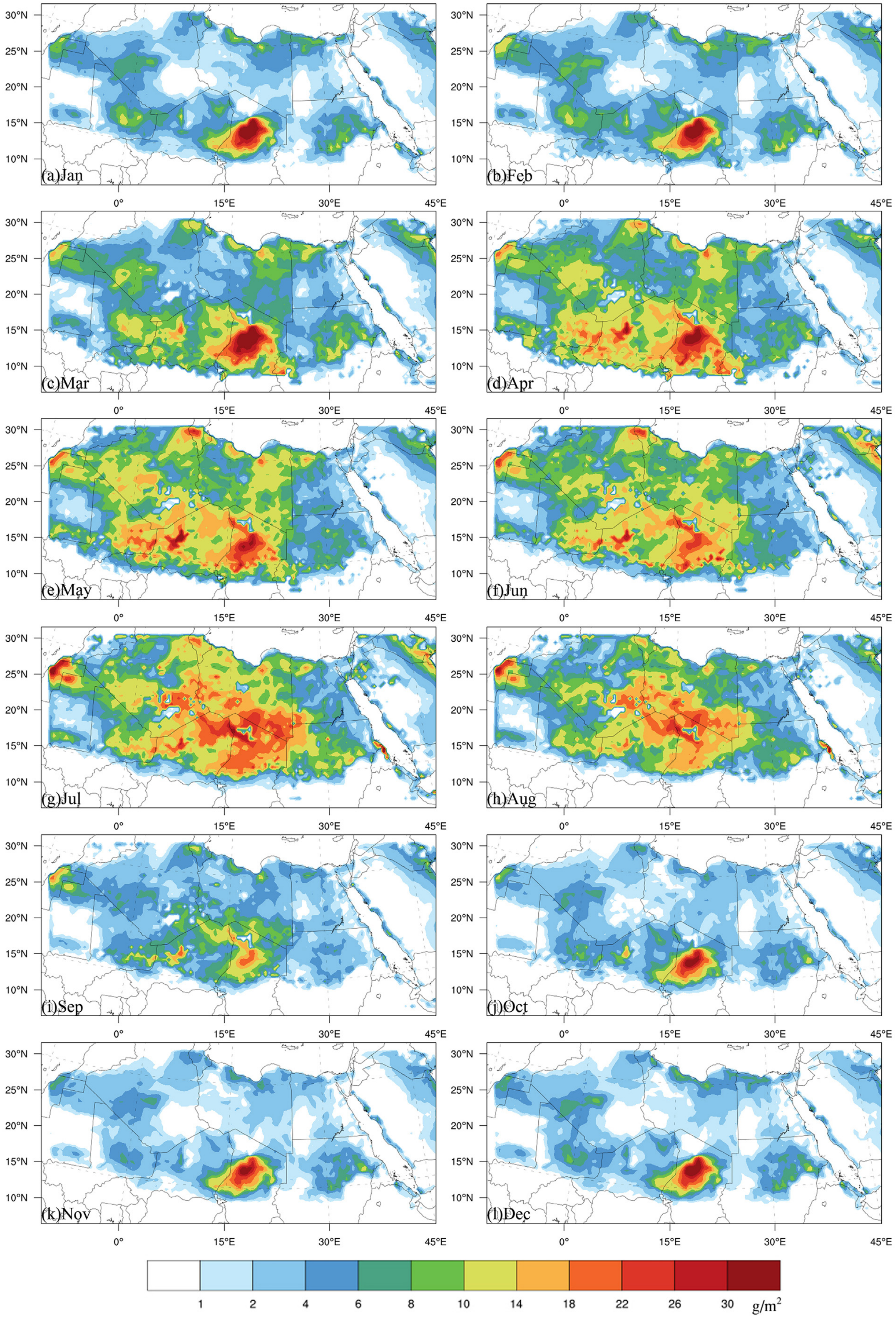

Fig. 7. Spatial distribution of monthly averages of sum of dust emission in North Africa from 1997 to 2016.

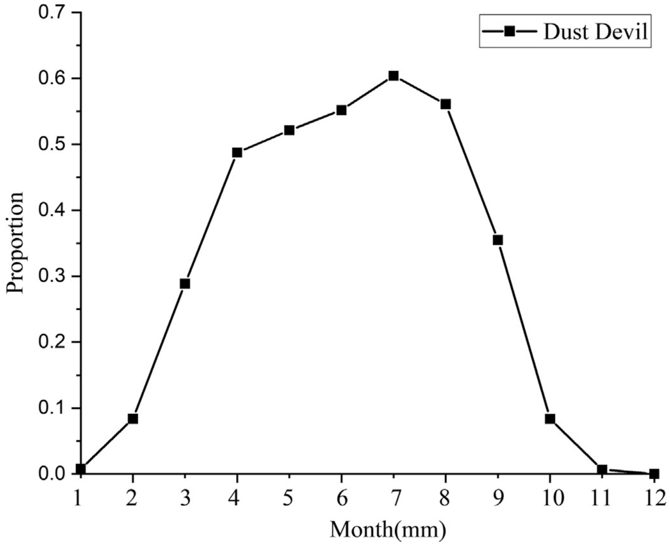

Fig. 8. Monthly mean of occurrence frequency of dust devils in North Africa from 1997 to 2016.

characteristics of AI, the AI also reflects the remote transport of dust aerosol to the local area as well as possibly new dust emission mechanisms that have not been discovered.

3.5. Contribution of dust devil to dust emission

The 20-year monthly average of the dust devils in North Africa shows a single-peak distribution (Fig. 8), with a near-zero contribution in the winter months, a sharp increase after February, a contribution >50% from April to August, reaching a maximum of 60% in July, a precip-itous decline after August, and almost zero after November.

Because dust devils occur most frequently from April to August, we use the spatial distribution of the dust devil's contribution in each month during this period to determine the dominant area of dust devils in North Africa. In order to study the contribution of dust devil to the sum of dust emission by dust storms and dust devils, the regions where dust devil contributes >50% are defined as dust devil dominant regions.

It is clear from Fig. 9a–e that the dust devil dominant areas extend northward from the Tibesti Plateau, the Hoggar Mountains, the west side of the Air Mountains, near the Atlas Mountains and the south side of the Calnascio Desert, and connect with the area near the Atlas Moun-tains, then expand eastward to the areas near the Red Sea. In April to May, the dominant regions are concentrated in the Atlas Mountains, Hoggar Mountains, Tibesti Plateau, south side of Calnascio Desert, and Sahel area to the south of 20°N (except Bodélé Depression and Nubian Desert). The spatial distribution of contribution from June to July is sim-ilar to that in May, but the contribution rate continues to increase and reach a maximum of >90% in the middle east region of North Africa (in-cluding the Edeyen Ubari, the Edeyen Murzuq, the Calnascio Desert, the

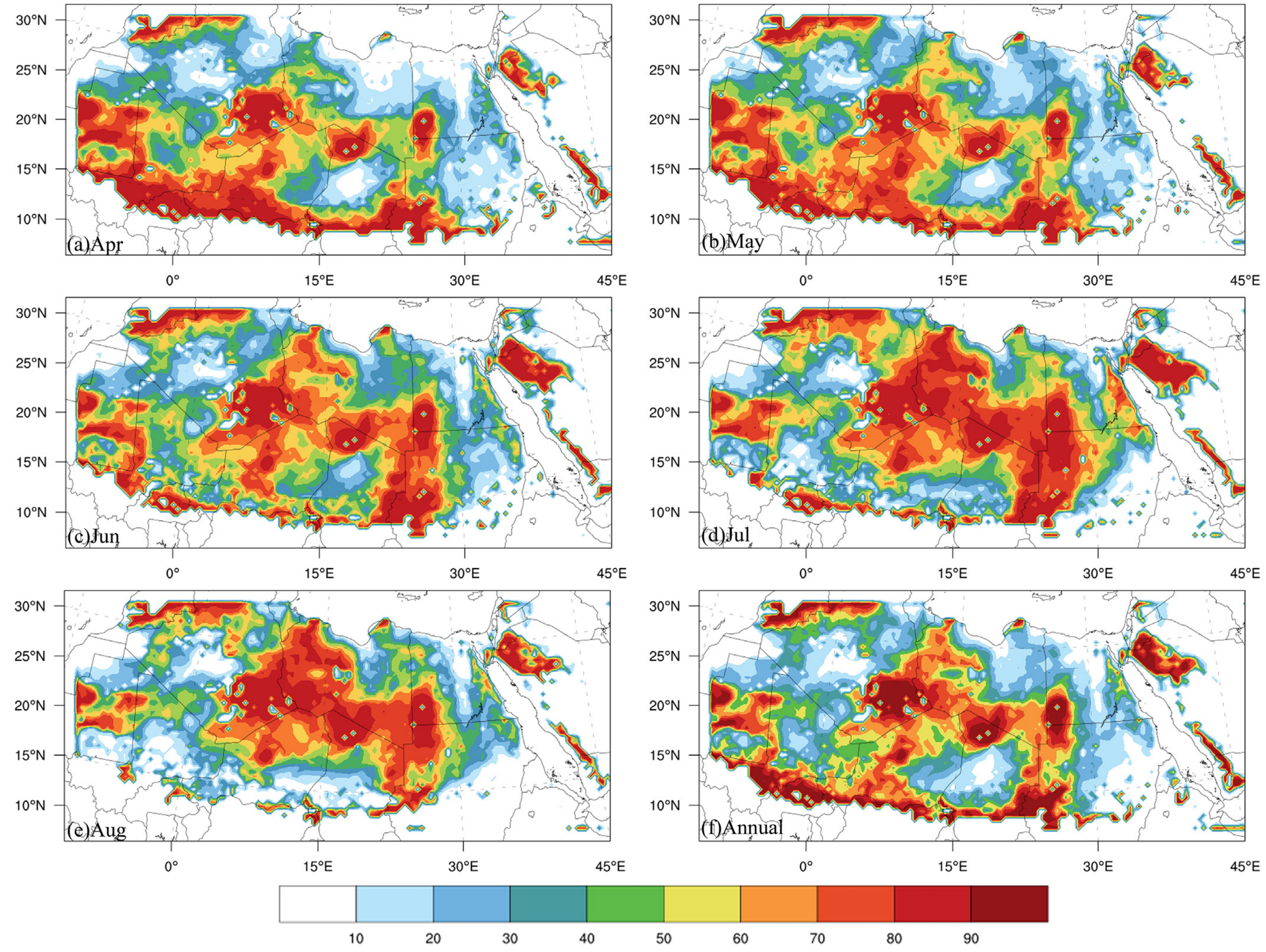

Fig. 9. Spatial distribution of mean and annual contribution rate of dust devil from April to August in North Africa form 1997 to 2016.

Libyan Desert, the Erg Rebiana and the Nubian Desert), while the contri-bution of the Red Sea coastal areas also increases significantly. The con-tribution of the 10–20°N area is further decreased to <60%, and the area with >90% contribution shrank to a narrow strip. In August, the contri-bution begins to decrease overall, with dominant regions shrinking to-wards central North Africa, mainly in the vicinity of the Hoggar Mountains, the Edeyen Murzuq, the Tibesti Plateau and the south side of Calnascio Desert. It is worth noting that even from April to August, when the contribution of dust devil is the largest, the contribution in Grand Erg Occidental and Bodélé Depression has been <40%, and the dominant dust emission mechanism in these areas is dust storm. After September, dust storm is the main dust emission mechanism in North Africa.

The 20-year average annual contribution shows more succinctly the dominant areas of dust storms and dust devils. Fig. 9f shows that the dust devil dominated areas are concentrated in Atlas Mountains, Hoggar Mountains, west of Maurit Desert - Djouf Desert - El Mréyé, Tibesti Pla-teau, near Air Mountains, south of Calnascio Desert, and south of 15°N in Sahel region, while the rest of the area is dominated by dust storm. In any case, the dust devil dominant area is significantly smaller than the dust storm dominant area, and the 20-year average annual contribution of 61.3% by dust storm, suggesting that the dust aerosol in North Africa is still dominated by dust storm. This finding is also confirmed by the 20-year average annual contribution of 38.7% from North Africa dust devil. Compared with previous studies, the contribution portion of dust devil is consistent with the previous findings of >30% in North African (Marsham et al., 2008) and 35% in the world(Koch and Renno, 2005), but lower than 53% in the northern deserts of China (Han et al., 2016).

4. Conclusions

Based on the combined analysis of AI, numerical simulations, and dust observations at the 300 meteorological stations for the same 20-year period, the similarities and differences in the spatio-temporal distributions of AI, dust storms, and dust devil emissions are investigated to determine the dust emission areas of dust storms and dust devils in North Africa. The main findings are summarized as follows.

1) North Africa dust storms mainly occur in Spring and their emission areas are mainly concentrated from the Grand Erg Occidental to the Erg Chech-Adrar, the northern part of the Grand Erg Oriental, the Mediterranean coast, the eastern side of Nubian Desert, the Atouila Desert to the Ouarane Desert, and Bodélé Depression.
2) Dust devils mainly occur from April to August, and their emission areas are mainly concentrated in the central part of North Africa, especially from the southwest of Hoggar Mountains to the west of Air Mountains, the border area of Egypt - Sudan - Libya and the vicinity of Tibesti Plateau.
3) The spatio-temporal distribution of AI is correlated more with that of dust devils than that of dust storms. However, most dust devils occur from April to August and the others months are dominated by dust storms, leading to an overall annual contribution of 61.3% by dust storms, only 38.7% by dust devil.

It is noteworthy that although the spatial distribution of AI and the sum of dust emission by dust storms and dust devils in each month are generally similar, detailed differences remain. The contribution from long-distance dust transports may be responsible for the remaining discrepancy, and thus merits further study in the future.

CRediT authorship contribution statement

Lin Pan: Investigation, Software, Formal analysis, Writing - Original Draft

Yongxiang Han: Ideas, formulation or evolution of overarching research goals and aims, Writing- Reviewing and Editing, Supervision

Zhengqi Lu: Software help, Validation, Data Curation
Jiaxin Li: Validation
Fei Gao: Resources
Zhaohuan Liu: Review & Editing
Weijia Liu: Validation
Yangang Liu: Writing - Review & Editing

Declaration of competing interest

We declare that we do not have any commercial or associative interest that represents a conflict of interest in connection with the work submitted. No conflict of interest exits in the submission of this manuscript, and manuscript is approved by all authors for publication. I would like to declare on behalf of my co-authors that the work described was original research that has not been published previously, and not under consideration for publication elsewhere, in whole or in part. All the authors listed have approved the manuscript that is enclosed.

Acknowledgements

This work is supported by the National Natural Science Foundation of China (No. 41875176), and the numerical simulations are done on the supercomputing system in the Supercomputing Center of Nanjing University of Information Science & Technology. Y. Liu is supported by the U.S. Department of Energy's Atmospheric System Research (ASR) program.

References

Alpert, P., Kaufman, Y.J., Shay-El, Y., et al., 1998. Quantification of dust-forced heating of the lower troposphere. Nature 395 (6700), 367–370. https://doi.org/10.1038/26456.

Ansmann, A., Tesche, M., Knippertz, P., et al., 2009. Vertical profiling of convective dust plumes in southern Morocco during SAMUM. Tellus Series B-chemical & Physical Meteorology 61 (1), 340–353. https://doi.org/10.1111/j.16000889.2008. 00384.x.

Balme, M., Greeley, R., 2006. Dust devils on Earth and Mars. Rev. Geophys. 44 (3), 1–22. https://doi.org/10.1029/2005RG000188.

Bertrand, J., Cerf, A., Domergue, J.L., 1979. Repartition in space and time of dust haze south of the Sahara. WMO. 538, 409–415.

Birkett, C.M., 2000. Synergistic remote sensing of Lake Chad: variability of basin inundation. Remote Sens. Environ. 72 (2), 218–236. https://doi.org/10.1016/S0034-4257(99)00105-4.

Brooks, N., Legrand, M., 2000. Dust variability over northern Africa and rainfall in the Sahel. Linking Climate Change to Land Surface Change 6, 1–25.

Evan, A.T., Fiedler, S., Zhao, C., et al., 2015. Derivation of an observation-based map of North African dust emission. Aeolian Res. 16, 153–162. https://doi.org/10.1016/j.aeolia.2015.01.001.

Gillette, D., Sinclair, P.C., 1990. Estimation of suspension of alkaline material by dust devils in the United States. Atmos. Environ. 24, 1135–1142. https://doi.org/10.1016/0960-1686(90)90078-2.

Goudie, A.S., Middleton, N.J., 2001. Saharan dust storms: nature and consequences. Earth Sci. Rev. 56 (1), 179–204. https://doi.org/10.1016/S0012-8252(01) 00067-8.

Gu, Z.L., Zhao, Y.Z., Yu, Y.Z., et al., 2003. Numerical study of the fomation evolution and structure of dust devil. Acta Meteorologica Sinica 61 (6), 751–760. https://doi.org/10.11676/qxxb2003.076.

Gu, Z.L., Wei, W., Zhao, Y.Z., 2010. An overview of surface conditions in numerical simulations of dust devils and the consequent near-surface air flow fields. Aerosol Air Qual. Res. 10 (3), 272–281. https://doi.org/10.4209/aaqr. 2009.12.0077.

Han, Y.X., Dai, X., Fang, X., et al., 2008. Dust aerosols: a possible accelerant for an increasingly arid climate in North China. J. Arid Environ. 72 (8), 1476–1489. https://doi.org/10.1016/j.jaridenv.2008.02.017.

Han, Y.X., Wang, K., Liu, F., et al., 2016. The contribution of dust devils and dusty devils to the aerosol budget in western China. Atmosphere Environment 126, 21–27. https://doi.org/10.1016/j.atmosenv.2015.11.025.

Helgren, D.M., Prospero, J.M., 1987. Wind velocities associated with dust deflation events in the Western Sahara. J. Appl. Meteorol. 26 (9), 1147–1151 doi:10.1175/1520-0450(1987)026<1147:WVAWDD>2.0.CO;2.

IPCC, 2013. Climate Change: The Physical Science Basis. Contribution of Working Group I to the Fifth Assessment Report of the Intergovernmental Panel on Climate Change. Cambridge University Press.

Jemmett-Smith, B.C., Marsham, J.H., Knippertz, P., et al., 2015. Quantifying global dust devil occurrence from meteorological analyses. Geophys. Res. Lett. 42 (4), 1275–1282. https://doi.org/10.1002/2015GL063078.

Kalu, A.E., 1979. The African dust devil: its characteristics and propagation across West Africa in winter. In: Morales, C. (Ed.), Saharan Dust: Mobilization, Transport, Deposition. John Wiley & Sons, New York, pp. 95–118.

Klose, M., Shao, Y., 2016. A numerical study on dust devils with implications to global dust budget estimates. Aeolian Res. 22, 47–58. https://doi.org/10.1016/j.aeolia.2016.05.003.

Koch, J., Renno, N.O., 2005. The role of convective devils and vortices on the global aerosol budget. Geophys. Res. Lett. 32 (18), L18806. https://doi.org/10.1029/2005GL023420.

Liu, Y., Han, Y.X., Yang, W.Q., et al., 2018. Impacts of sand weathers and dust devils on the local dust emission amount. J. Desert Res. 38 (6), 1175–1179.

Lyons, T., Nair, U., Foster, I., 2008. Clearing enhances dust devil formation. J. Arid Environ. 72 (10), 1918–1928. https://doi.org/10.1016/j.jaridenv.200 8.05.009.

Mahowald, N.M., Zender, C.S., Luo, C., et al., 2002. Understanding the 30-year Barbados desert dust record. J. Geophys. Res.. 107 (D21), art. no.-4561. doi:https://doi.org/10.1029/2002JD002097.

Maley, J., 1982. Dust, clouds, rain types and climatic variations in tropical North Africa. Quat. Res. 18 (1), 1–16. https://doi.org/10.1016/0033-5894(82) 90018-7.

Marsham, J.H., Parker, D.J., Grams, C.M., et al., 2008. Observations of mesoscale and boundary-layer scale circulations affecting dust transport and uplift over the Sahara. Atmos. Chem. Phys. 8 (23), 6979–6993. https://doi.org/10.5194/acp-8-6979-2008.

Martin, J.H., 1990. Glacial-interglacial CO_2 change: the iron hypothesis. Paleoceanography 199 (5), 1–13. https://doi.org/10.1029/PA005i001p00001.

Metzger, S.M., 1999. Dust Devils as Aeolian Transport Mechanisms in Southern Nevada and the Mars Pathfinder Landing Site. Thesis. University of Nevada, p. 744 1999.

Mokhtari, M., Tulet, P., Fischer, C., et al., 2015. Three-dimensional dust aerosol distribution and extinction climatology over northern Africa simulated with the ALADIN numerical prediction model from 2006 to 2010. Atmos. Chem. Phys. 15, 9063–9082. https://doi.org/10.5194/acp-15-9063-201 5.

N'Tchayi, M.G., Berrand, J.J., Nicholson, S.E., 1997. The diurnal and seasonal cycles of wind-borne dust over Africa north of the Equator. J. Appl. Meteorol. 36 (7), 868–882 doi: 10.1175/1520-0450(1997)036< 0868:TDASCO>2.0.CO;2.

Obianyo, J.I., 2019. Effect of salinity on evaporation and the water cycle. Emerging Science Journal 3 (4), 255–262. https://doi.org/10.28991/esj-2019-01188.

Oke, A., Tapper, N., Dunkerley, D., 2007. Willy-willies in the Australian landscape: the role of key meteorological variables and surface conditions in defining frequency and spatial characteristics. J. Arid Environ. 71 (2), 201–215. https://doi.org/10.1016/j.jaridenv.2007.03.008.

Oo, H.T., Zin, W.W., Kyi, C.C.T., 2019. Assessment of future climate change projections using multiple global climate models. Civil Engineering Journal 5 (10), 2152–2166. https://doi.org/10.28991/cej-2019-03091401.

Pan, L., Han, Y.X., Lu, Z.Q., et al., 2020. Temporal and spatial distribution and long-range transport pathway of dust weather in North Africa. China Environ. Sci. 40 (1), 76–84.

Perlwitz, J., Tegen, I., Miller, R.L., 2001. Interactive soil dust aerosol model in the GISS GCM 1. Sensitivity of the soil dust cycle to radiative properties of soil dust aerosols. J. Geophys. Res. 106 (16), 18167–18192. hdoi:https://doi.org/10.1029/2000JD900668.

Prospero, J.M., Ginoux, P., Torres, O., et al., 2002. Environmental characterization of global sources of atmospheric soil dust identified with the Nimbus 7 Total Ozone Mapping Spectrometer (TOMS) absorbing aerosol product. Rev. Geophys. 40 (1). https://doi.org/10.1029/2000RG000095 2(1-31).

Ridgwell, A.J., 2007. Dust in the Earth system: the biogeochemical linking of land, air and sea. Adv. Earth Science, 51–68 https://doi.org/10.1098/rsta.2002.109 6.

Sinclair, P.C., 1969. General characteristics of dust devils. J. Appl. Meteorol. 8 (1), 32–45. https://doi.org/10.1175/1520-0450(1969)008<0032:G CODD>2.0.CO;2.

Solangi, G.S., Siyal, A.A., Siyal, P., 2019. Spatiotemporal dynamics of land surface temperature and its impact on the vegetation. 5 (8), 1753–1763. https://doi.org/10.28991/cej-2019-03091368.

Tang, Y.G., Han, Y.X., Liu, Z.H., 2018. Temporal and spatial characteristics of dust devils and their contribution to the aerosol budget in East Asia. Atmos. Environ. 182, 225–233. https://doi.org/10.1016/j.atmosenv.2018.03.050.

Wang, Y.Q., Stein, A.F., Draxler, R.R., et al., 2011. Global sand and dust storms in 2008: observation and HYSPLIT model verification. Atmos. Environ. 45, 6368–6381. https://doi.org/10.1016/j.atmosenv.2011.08.035.

Wang, M.J., Han, Y.X., Deng, Z.Q., et al., 2012. Relationship between dust aerosols and solar radiation in global dust source regions. China Environ. Sci. 32 (4), 577–583. https://doi.org/10.1007/s11783-011-0280-z.

Wang, W.C., Sheng, L.F., Jin, H.C., et al., 2015. Dust aerosol effects on cirrus and altocumulus clouds in Northwest China. Journal of Meteorological Research 29 (5), 793–805. https://doi.org/10.1007/s13351-015-4116-9.

Washington, R., Todd, M.C., Middleton, N.J., et al., 2003. Dust-storm source areas determined by the total ozone monitoring spectrometer and surface observations. Ann. Assoc. Am. Geogr. 93 (2), 297–313. https://doi.org/10.1111/1467-8306.9302003.

Watson, A.J., Bakker, D.C.E., Ridgwell, A.J., et al., 2000. Effect of iron supply on Southern Ocean CO_2 uptake and implications for glacial atmospheric CO_2. Nature 407 (6805), 730–733. https://doi.org/10.1038/35037561.